Journal of Materials Chemistry A

An asymmetrical A-DAD-A-Type Acceptor Simultaneously Enhances Voltage and Current for Efficient Organic Solar Cells

Journal:	*Journal of Materials Chemistry A*
Manuscript ID	TA-ART-03-2020-003128.R1
Article Type:	Paper
Date Submitted by the Author:	26-Apr-2020
Complete List of Authors:	Lai, Hanjian; Southern University of Science and Technology, Chemistry Chen, Hui; Southern University of Science and Technology, Chemistry Zhu, Yulin; Southern University of Science and Technology, Chemistry Chen, Lin; Southern University of Science and Technology, Chemistry Huang, Hsin-Hsiang; National Taiwan University He, Feng; Southern University of Science and Technology, Chemistry

ARTICLE

An asymmetrical A-DAD-A-Type Acceptor Simultaneously Enhances Voltage and Current for Efficient Organic Solar Cells

Hanjian Lai, [‡,a, b] Hui Chen, [‡,a] Yulin Zhu, [a] Lin Chen, [a] Hsin-Hsiang Huang, [d] and Feng He[*a, c]

[a] Shenzhen Grubbs Institute and Department of Chemistry, Southern University of Science and Technology, Shenzhen 518055, China

[b] School of Chemistry and Chemical Engineering, Harbin Institute of Technology, Harbin, 150001, China

[c] Guangdong Provincial Key Laboratory of Catalysis, Southern University of Science and Technology, Shenzhen 518055, China

[d] Department of Materials Science and Engineering, and Center for Condensed Matter Sciences, National Taiwan University, Taipei 10617, Taiwan

‡ These authors contributed equally

* E-mail: hef@sustech.edu.cn (F.H.)

Table of contents entry

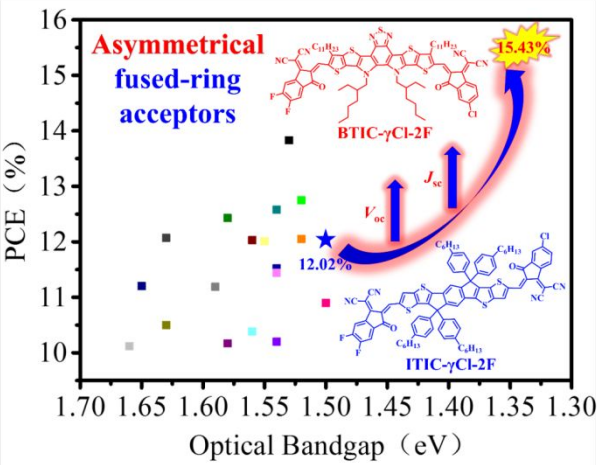

This work provides a strategy of symmetry breaking in an A-DAD-A-type acceptor with a PCE of 15.43%, which is the highest value reported to date for asymmetrical fused-ring acceptors.

Abstract

The asymmetrical molecule is a promising class of fused-ring electron acceptor (FREA) for use in organic solar cells (OSCs). Hence, two molecules were synthesized to compare the differences between A-D-A (acceptor-donor-acceptor)-type and A-DAD-A (acceptor-donor-acceptor-donor-acceptor)-type asymmetrical acceptors, named **ITIC-γCl-2F** and **BTIC-γCl-2F**, respectively. **BTIC-γCl-2F** exhibits larger dipole moments (μ_m) and a red-shifted absorption, which would be beneficial in obtaining a greater short-circuit current (J_{sc}). After they were fabricated as OSC devices, an extremely large increase in J_{sc} was achieved in **BTIC-γCl-2F**-based devices without a decrease in the open circuit voltage (V_{oc}); one important reason for this phenomenon is that the introduction of nitrogen atoms in the core of **BTIC-γCl-2F** can effectively increase the HOMO energy level but with little change in the LUMO energy level. Consequently, devices based on **BTIC-γCl-2F** achieve a champion power conversion efficiency (PCE) of 15.43%, which is the highest value reported to date for asymmetrical acceptor-based OSCs. The more obvious fibrillar network and more homogeneous morphology of **BTIC-γCl-2F** leads to faster electron and hole mobilities, which is consistent with higher J_{sc} and fill factor (FF). This suggests hat A-DAD-A-type symmetry breaking is a promising strategy that can be used for designing high-performance asymmetrical FREAs.

Introduction

Polymer solar cells (OSCs) are one of the most convenient and promising photovoltaic technologies for their advantages of lightweight, solution processability, flexibility, and semitransparency[1-4]; the PCEs for converting light energy into electricity have rapidly exceeded 16%[5, 6]. The bulk heterojunction is considered to be the state-of-the-art OSC structure, comprising a blend of donors and acceptors, in which acceptors can be categorized into fullerene acceptors and FREAs[7]. In the past twenty years, fullerene

acceptors have been widely used, with the PCEs for fullerene derivative based single junction OSC devices exceeding 11% but not exceeding 12%[8-10]. In comparison, the emergence of FREAs, including A-D-A-type and A-DAD-A-type small molecules, has eliminated this bottleneck. OSC devices based on A-D-A-type FREAs exhibit PCEs of over 13%; the most widely used molecule is IT-4F[11], and A-DAD-A-type FREA-based OSC devices represented by Y6[12] have achieved PCEs of over 15%. The high performance of FREAs is due to their good solubility, appropriate crystallinity, fine-tuned morphology, matched absorption spectra and energy levels achieved through backbone engineering[13, 14], side-chain strategies[15, 16], and end-group modifications[17, 18].

The asymmetrical design provides an alternative idea for the development of FREA materials; the PCEs for devices based on asymmetrical acceptors have increased rapidly from less than 1% to more than 13% in the last 10 years[19]. The advantages of asymmetric modification, such as larger dipole moments and stronger intermolecular bonding energy, have attracted the attention of many researchers[20]. Initially, the asymmetrical fullerene acceptors $PC_{71}BM$ and $PC_{61}BM$ were widely used, making important contributions to the rise and development of OSCs[21, 22]. Subsequently, many researchers have focused on the exploration of asymmetrical FREAs, especially A-D-A-type asymmetrical FREAs. For example, firstly, developing asymmetrical cores to adjust the size of backbones and the electron-rich abilities,[23, 24] Yang et al. reported an asymmetrical core-based acceptor, named IDTCN (μ_m=4.51 D), while the symmetric core-based acceptors IDTCN and ITCPTC exhibit low dipole moments of 0 and 0.07 D, respectively, thus, IDTCN-based devices show a higher FF of 73.77% than its counterparts due to its higher electron/hole mobilities and balanced charge mobilities. Secondly, designing asymmetrical side chains and end groups to regulate intermolecular packings and intermolecular interactions, [25-28] Bo et al. synthesized an acceptor with asymmetric side chains, IDT-OB, which possesses better solubility and more ordered molecular packings. Therefore, it affords a favorable phase separation and balanced charge mobilities, resulting in a higher PCE of 10.12%. However, symmetry breaking in A-DAD-A-type FREAs has barely been investigated, and more attention should be paid to such high-performance systems for

understanding the differences between A-D-A-type asymmetrical FREAs and A-DAD-A-type asymmetrical FREAs.

Thus, in this work, an A-D-A-type asymmetrical FREA and an A-DAD-A-type asymmetrical FREA were designed and synthesized, named **ITIC-γCl-2F** and **BTIC-γCl-2F,** respectively. Density function theory (DFT) calculation revealed that the two molecules have good planarity with small dihedral angles between the cores and end groups, while the end groups are distributed on the opposite side of the backbone for **ITIC-γCl-2F** and on the same side for **BTIC-γCl-2F**. The dipole moments for **ITIC-γCl-2F** and **BTIC-γCl-2F** were determined to be 1.05 D and 1.54 D, respectively; the larger dipole moment of **BTIC-γCl-2F** can benefit intermolecular charge migration[29]. In addition, **ITIC-γCl-2F** and **BTIC-γCl-2F** exhibit higher dipole moments than its corresponding symmetrical counterparts, respectively, indicating that the symmetry breaking is an effective way to increase the dipole moments of molecules in both A-D-A- and A-DAD-A-type systems. Compared to **ITIC-γCl-2F**, **BTIC-γCl-2F** possesses redshifted absorption spectra with a maximum absorption peak at 818 nm in pristine films, and an absorption edge located at 918 nm, corresponding to an optical bandgap of 1.35 eV. An electrochemical test indicated that a much higher HOMO energy level is present in **BTIC-γCl-2F**, while there is not much difference in the LUMO energy level, which can be explained by the fact that the introduction of nitrogen atoms into the core of **BTIC-γCl-2F** can effectively increase the HOMO energy level of the molecule[30, 31]. This should be one of the reasons why A-DAD-A-type asymmetrical FREAs show more redshifted absorptions but still maintain a higher V_{oc} than A-D-A-type asymmetrical FREAs. After their fabrication as OSC devices, **BTIC-γCl-2F**-based devices show a V_{oc} of 0.86 eV and J_{sc} of 24.60 mA cm^{-2}, corresponding to a PCE of up to 15.43%, which is 28.4% higher than that of the **ITIC-γCl-2F**-based device. It should be noted that the PCE value of 15.43% is the highest value obtained for asymmetrical FREA-based devices[23], thus, the asymmetric modification should be an efficient way to regulate the molecular properties and improve the performance of it. The electron and hole mobilities measured by the SCLC method are also consistent with the higher J_{sc} found by *J-V* test for OSC devices based on **BTIC-**

γCl-2F. These results provide a feasible strategy for designing high-performance asymmetrical FREAs via A-DAD-A-type symmetry breaking; compared with the A-D-A-type analog, A-DAD-A-type asymmetrical FREAs exhibit great application values and development potential.

Result and Discussion

The two small asymmetrical molecules were obtained by one-step synthesis according to the Knoevenagel condensation reaction with IT-2CHO and BT-2CHO cores[32]. After purification by a silica-gel column and HPLC, **ITIC-γCl-2F** and **BTIC-γCl-2F** were obtained with yields of 37.0% and 39.1%, respectively; details can be found in the supplementary information. Common solvents such as toluene, chloroform, and chlorobenzene can dissolve these two asymmetrical molecules well, indicating that both of the molecules meet the conditions for solution processing. Differential scanning calorimetry (DSC) and thermogravimetric (TGA) analysis were used to measure the thermal properties of the two asymmetrical molecules, and the corresponding curves are shown in **Figure S1** and **Figure S2**. **ITIC-γCl-2F** and **BTIC-γCl-2F** show good thermal stabilities, with 5%-weight-loss temperatures (T_d) of 314°C and 324°C, respectively, and no obvious peak observed in the DSC traces, both molecules meet the thermal requirements as acceptors in active layers for OSC devices.

Figure 1 shows the chemical structures for **ITIC-γCl-2F** and **BTIC-γCl-2F** and their configurations as visualized by B3LYP/6-31G (d, p) DFT calculation. This figure shows that both molecules have good planarity with small dihedral angles between cores and end groups: 0.08°/0.06° for **ITIC-γCl-2F** and 0.36°/0.43° for **BTIC-γCl-2F**. However, there are some differences in molecular configurations between the two asymmetrical molecules. In detail, **ITIC-γCl-2F** exhibits a Z-type structure with the end groups distributed on the opposite side of the backbone, and the four phenylhexyl side chains are distributed on two sides of the center cores in the form of sp^3 hybridization, which can hinder the packing of cores due to steric effects, resulting in the existence of only π-π stacking between end groups to form typical J-aggregations[33]. On the other hand, the end groups are on the same side of the backbone for **BTIC-γCl-2F**,

which compose a Y-type structure. The alkyl chains with smaller steric hindrance are on the one side of the benzothiadiazole, which provides a chance for the center cores to be packed to some extent. Thus, cooperating H/J-aggregation should be found in **BTIC-γCl-2F**[34]. **Figure S6** indicates that the calculated HOMO energy levels for **ITIC-γCl-2F** and **BTIC-γCl-2F** are -5.58 eV and -5.57 eV, which mainly distribute along the backbones, and the calculated LUMO energy level for **ITIC-γCl-2F** is delocalized across the whole molecule with a value of -3.49 eV, while the calculated LUMO energy level for **BTIC-γCl-2F** is -3.54 eV with a distribution tending towards the end groups. Differences in the LUMO energy level distribution can affect the dipole moment of molecules. Consequently, the dipole moments for **ITIC-γCl-2F** and **BTIC-γCl-2F** are calculated to be 1.05 D and 1.54 D, respectively. The larger dipole moment of **BTIC-γCl-2F** can benefit intermolecular charge mobility. The dipole moments of the corresponding symmetrical molecules **ITIC-4F** and **Y6** were also provided to give insights regarding the distinctive properties of the asymmetric modification, which was shown in **Figure S3**. Compared to its counterpart, **ITIC-4F** exhibit a lower μ_m of 0.19 D and a μ_m of 0.87 D was found in **Y6** [35]. Those results indicate that the symmetry breaking is an effective way to increase the dipole moments of molecules in both A-D-A- and A-DAD-A-type systems.

A UV-Vis absorption test was used to investigate the optical properties of the two asymmetrical FREAs. **Figure 2a** shows the solution UV-Vis absorption spectra for **ITIC-γCl-2F** and **BTIC-γCl-2F** with maximum peaks identified at 691 nm and 731 nm, respectively; the extinction coefficients for the two asymmetrical molecules in chloroform are 2.43×10^5 L mol^{-1} cm^{-1} and 1.33×10^5 L mol^{-1} cm^{-1}, respectively. **ITIC-γCl-2F** shows a higher solution extinction coefficient but blue-shifted absorption. In addition, the symmetrical molecules **ITIC-4F** and **Y6** were used to compare the optical properties of symmetric counterparts and the asymmetric ones. The solution extinction coefficients of **ITIC-4F**[11] and **Y6**[12] are 2.10×10^5 and 1.07×10^5 L mol^{-1} cm^{-1}, respectively, which is both lower than that of their corresponding analogies, indicating the asymmetric modification in A-D-A- and A-DAD-A-type acceptors by the introduction of chlorine atom on terminal units can significantly enhance ICT effect and

increase solution extinction coefficient, which is consistent with higher polarities of asymmetric acceptors. The neat film absorptions are shown in **Figure 2b**, and the normalized absorptions are shown in **Figure S4**; in detail, **ITIC-γCl-2F** exhibits an absorption wavelength range of 550~800 nm with an absorption coefficient of 8.11×10^4 cm^{-1}, while a wider wavelength range of 550~900 nm was realized for the **BTIC-γCl-2F** film. Compared to A-D-A-type **ITIC-γCl-2F**, the A-DAD-A-type **BTIC-γCl-2F** possesses a larger absorption coefficient of 1.06×10^5 cm^{-1} and a redshifted absorption with a maximum peak of 818 nm; this is good for sunlight harvesting to obtain higher J_{sc}. The absorptions for blend films were also determined. As shown in **Figure 2c**, the absorption of the **BTIC-γCl-2F**-blend film covers the absorption of the **ITIC-γCl-2F**-blend film and shows an additional strong absorption over the wavelength range from 730 nm to 850 nm; this result indicates that the absorption of **BTIC-γCl-2F** is better matched with the polymer donor. The electrochemical properties were determined by a cyclic voltammetry (CV) test; the energy level values are shown in **Figure 2d**, and the corresponding CV curves are shown in **Figure S5**. The polymer PBDB-TF was chosen as donor with LUMO and HOMO energy levels of -3.65 and -5.45 eV[17], respectively, the LUMO energy differences between PBDB-TF and acceptors provide enough driven force for charge separation. The LUMO and HOMO energy levels for **ITIC-γCl-2F** and **BTIC-γCl-2F** were determined to be -3.88 eV and -3.87 eV, and -5.52 eV and -5.39 eV, respectively. The much higher HOMO energy level of **BTIC-γCl-2F** can be explained by the fact that the introduction of nitrogen atoms into the core of **BTIC-γCl-2F** can effectively increase the HOMO energy level of the molecule. This should be one of the reasons why the A-DAD-A-type asymmetrical FREA shows more redshifted absorptions but still maintains a LUMO energy level with little changes compared to the A-D-A-type asymmetrical FREA. This result provides an idea for designing A-DAD-A-type asymmetrical FREAs rather than designing A-D-A-type asymmetrical FREAs and might be a way to challenge the trade-off between J_{sc} and V_{oc} via the enhancement of J_{sc} without much sacrifice of the V_{oc}.

To visualize the application values for the two asymmetrical molecules, inverted OSC devices were fabricated, where PBDB-TF was chosen as the polymer donor[35, 36]; the PBDB-TF structure is shown in

Scheme S2, and the specific device preparation processes are summarized in the supplementary information. As shown by the *J-V* curves in **Figure 3a**, the OSC devices based on **ITIC-γCl-2F** show a PCE of 12.02% with a V_{oc} of 0.85 V, a J_{sc} of 19.60 mA cm^{-2}, and a fill factor (FF) of 72.20%, while a higher V_{oc} of 0.86 V, J_{sc} of 24.60 mA cm^{-2}, and FF of 72.67% were realized for **BTIC-γCl-2F**-based OSCs devices, corresponding to a superior PCE of up to 15.43%. The A-D-A-type **ITIC-γCl-2F** achieved a V_{oc} of 0.85 V which is higher than 0.83 V of its symmetric counterpart ITIC-4F[37], while the same phenomenon was observed in A-DAD-A-type acceptors. This result implies the asymmetric modification induced by chlorination in both A-D-A- and A-DAD-A-type system could afford higher V_{oc} in OSC devices, and the asymmetric modification should be an efficient way to regulate the molecular properties and further improve their device performance. The better performance in V_{oc} and J_{sc} meets the prior analysis of the optical and electrochemical properties of **BTIC-γCl-2F**. It is noteworthy that the PCE of 15.43% is the highest value obtained to date for asymmetrical acceptor-based OSC devices; asymmetrical acceptors reported in the literature with PCEs of over 10% are summarized in **Figure 3c**[19, 23]. **Figure 3b** shows the external quantum efficiency (EQE) curves obtained for the two asymmetrical molecule-based OSC devices, with a strong photoresponse observed from 400 nm to 800 nm, while an extra photoresponse over the wavelength range of 750~900 nm was found for **BTIC-γCl-2F**-based devices benefiting from the extended spectra, resulting in a calculated J_{cal} of 23.78 mA cm^{-2} which is much higher than the value of 18.65 mA cm^{-2} produced by the **ITIC-γCl-2F** based device. It seems that compared to designing and synthesizing A-D-A-type asymmetrical molecules, designing and synthesizing A-DAD-A-type asymmetrical molecules should be more promising for developing high-performance devices in the asymmetrical OSC field.

The charge generation and dissociation properties of **ITIC-γCl-2F** and **BTIC-γCl-2F** were investigated by plotting the effective voltage (V_{eff}) versus the photocurrent density (J_{ph}); these curves are shown in **Figure 4a**. The **ITIC-γCl-2F** and **BTIC-γCl-2F**-based OSC devices show calculated charge dissociation probabilities of 0.95 and 0.96, respectively, under short-circuit conditions, which implies

more efficient charge dissociation in devices based on **BTIC-γCl-2F**. Furthermore, **Figure 4b** shows P (J_{sc} as a function of light density) versus J_{sc} curves for **ITIC-γCl-2F** and **BTIC-γCl-2F**-based OSC devices, where the slope values are both 0.97, indicating that bimolecular recombination behavior is suppressed in both asymmetrical FREA-based devices. The SCLC method was used to determine the charge transport properties of the two asymmetrical FREAs, and the electron and hole mobilities determined for **ITIC-γCl-2F** and **BTIC-γCl-2F**-based devices are shown in **Figure 4c** and **Figure 4d**, respectively. The electron mobilities for **BTIC-γCl-2F** and **ITIC-γCl-2F**-based OSC devices were calculated to be 1.8×10^{-4} cm^2 V^{-1} s^{-1} and 1.1×10^{-4} cm^2 V^{-1} s^{-1}, respectively, while the hole mobilities were 2.6×10^{-4} cm^2 V^{-1} s^{-1} and 1.7×10^{-4} cm^2 V^{-1} s^{-1}, respectively. The reason why **BTIC-γCl-2F** possesses higher mobilities than that of **ITIC-γCl-2F** should be explained by the relationship between A-D-A- and A-DAD-A-type acceptors: in the previous work, researchers found there were not only π-π stacking interactions between end groups, but also strong intermolecular interactions between deficient cores in A-DAD-A-type acceptors, while there is only channel for electronic hopping between end groups in A-D-A-type acceptors. The cooperative H/J aggregations of A-DAD-A-type acceptors provide more transport nodes for charge transfer, thus, **BTIC-γCl-2F**-based blend film has higher mobilities than its counterpart **ITIC-γCl-2F**. In summary, the **BTIC-γCl-2F**-based devices show higher and balanced mobilities, and stronger charge dissociation abilities, leading to higher J_{sc} and FF compared to the **ITIC-γCl-2F**-based OSC devices.

The morphologies of **ITIC-γCl-2F** and **BTIC-γCl-2F**-based blend films were characterized by transmission electron microscopy (TEM) and atomic force microscopy (AFM) tests, respectively. As shown in **Figure 5a** and **Figure 5b**, the **ITIC-γCl-2F** and **BTIC-γCl-2F** blend films feature a root mean square (RMS) of 1.76 nm and 1.07 nm, respectively, implying a smoother and more uniform morphology in **BTIC-γCl-2F** blend films. In addition, **Figure 5c** and **Figure 5d** indicate that **BTIC-γCl-2F** blend films possess a more obvious fibrillar network than that of **ITIC-γCl-2F**. Thus, **BTIC-γCl-2F** blend films feature a better phase separation for charge transport, resulting in superior electron and hole mobilities.

To further investigate the molecule packing information in devices, **ITIC-γCl-2F** and **BTIC-γCl-2F**-based neat films and blend films were characterized by grazing-incidence wide-angle X-ray scattering (GIWAXS) tests; **Figure S7** shows the line-cuts for the in-plane (IP) and out-of-plane (OOP) directions, and the corresponding 2D patterns are shown in **Figure S8**. Both molecules exhibit scattering peaks at around q_z = 1.66 $Å^{-1}$ in the OOP direction, indicating a priority for face-on orientation in **ITIC-γCl-2F** and **BTIC-γCl-2F** films. The scattering peaks at 0.31 and 0.30 $Å^{-1}$ in the IP direction correspond to lamellar structures with periods of 20.3 Å and 20.9 Å for **ITIC-γCl-2F** and **BTIC-γCl-2F**, respectively. After blending with the donor, the PBDB-TF: **ITIC-γCl-2F** and PBDB-TF: **BTIC-γCl-2F** blend films show scattering peaks at 1.63 $Å^{-1}$ and 1.62 $Å^{-1}$ in the OOP direction with π-π distances of 3.85 Å and 3.87 Å, respectively, implying that the two films also adopt the dominated face-on orientation, which is good for charge transport in devices.

Conclusions

In summary, two asymmetrical molecules, **ITIC-γCl-2F** and **BTIC-γCl-2F**, were used for fabricating OSC devices. The **BTIC-γCl-2F**-based devices achieve a PCE of 15.43% with simultaneous increases in J_{sc} and V_{oc}, which is 28.4% higher than that obtained for **ITIC-γCl-2F**-based OSC devices. Remarkably, this is the highest efficiency reported in the asymmetrical OSC field. The high-performance of A-DAD-A-type asymmetrical **BTIC-γCl-2F** can be credited to its larger dipole moments, red-shifted absorption, higher LUMO energy level, moderate phase separation, and superior electron and hole mobilities. In general, designing and synthesizing A-DAD-A-type asymmetrical molecules should be a more promising route for developing high-performance devices in the asymmetrical OSC field.

Conflicts of interest

There are no conflicts to declare.

Acknowledgments

This work was financially supported by the National Natural Science Foundation of China (21733005, 51773087, 21975115), Shenzhen Fundamental Research Program (KQJSCX20180319114442157, JCYJ20180302180238419, JCYJ20170817111214740), Shenzhen Nobel Prize Scientists Laboratory Project (C17213101), Guangdong Provincial Key Laboratory of Catalysis (No. 2020B121201002), Guangdong Innovative and Entrepreneurial Research Team Program (2016ZT06G587) and the Shenzhen Sci-Tech Fund (KYTDPT20181011104007). We thank Dr. Joseph Strzalka and Dr. Zhang Jiang for the assistance with GIWAXS measurements. Use of the Advanced Photon Source (APS) at the Argonne National Laboratory was supported by the U.S. Department of Energy, Office of Science, Office of Basic Energy Sciences, under contract No. DE-AC02-06CH11357. We also thank the SUSTech Core Research Facilities for the AFM and TEM measurements.

Notes and references

1. J. J. M. Halls, C. A. Walsh, N. C. Greenham, E. A. Marseglla, R. H. Frlend, S. C. Morattl and A. B. Holmes, *Nature*, 1995, **376**, 498-500.
2. G. Yu, J. Gao, J. C. Hummelen, F. Wudl, and A. J. Heeger, *Science*, 1995, **270**, 1789-1791.
3. G. Li, R. Zhu and Y. Yang, *Nat. Photonics*, 2012, **6**, 153-161.
4. A. J. Heeger, *Adv. Mater*., 2014, **26**, 10-28.
5. K. Jiang, Q. Wei, J. Y. L. Lai, Z. Peng, H. K. Kim, J. Yuan, L. Ye, H. Ade, Y. Zou and H. Yan, *Joule*, 2019, **3**, 3020-3033.
6. L. Hong, H. Yao, Z. Wu, Y. Cui, T. Zhang, Y. Xu, R. Yu, Q. Liao, B. Gao, K. Xian, H. Y. Woo, Z. Ge and J. Hou, *Adv. Mater*., 2019, **31**, 1903441.
7. C. B. Nielsen, S. Holliday, H. Y. Chen, S. J. Cryer and I. McCulloch, *Acc. Chem. Res*., *Accounts of*

chemical research, 2015, **48**, 2803-2812.

8. Y. Liu, J. Zhao, Z. Li, C. Mu, W. Ma, H. Hu, K. Jiang, H. Lin, H. Ade and H. Yan, *Nat. commun.*, 2014, **5**, 5293.
9. Z. He, B. Xiao, F. Liu, H. Wu, Y. Yang, S. Xiao, C. Wang, T. P. Russell and Y. Cao, *Nat. Photonics*, 2015, **9**, 174-179.
10. J. Zhao, Y. Li, G. Yang, K. Jiang, H. Lin, H. Ade, W. Ma and H. Yan, *Nat. Energy,* 2016, **1**, 15027-15033.
11. W. Zhao, S. Li, H. Yao, S. Zhang, Y. Zhang, B. Yang and J. Hou, *J. Am. Chem. Soc.*, 2017, **139**, 7148-7151.
12. J. Yuan, Y. Zhang, L. Zhou, G. Zhang, H.-L. Yip, T.-K. Lau, X. Lu, C. Zhu, H. Peng, P. A. Johnson, M. Leclerc, Y. Cao, J. Ulanski, Y. Li and Y. Zou, *Joule*, 2019, **3**, 1140-1151.
13. Y. Ma, M. Zhang, Y. Tang, W. Ma and Q. Zheng, *Chem. Mater.*, 2017, **29**, 9775-9785.
14. Z. Xiao, X. Jia, D. Li, S. Wang, X. Geng, F. Liu, J. Chen, S. Yang, T. P. Russell, and L. Ding, *Sci. Bull.*, 2017, **62**, 1562-1564.
15. Y. Li, N. Zheng, L. Yu, S. Wen, C. Gao, M. Sun and R. Yang, *Adv. Mater.*, 2019, **31**, 1807832.
16. J. Wang, W. Wang, X. Wang, Y. Wu, Q. Zhang, C. Yan, W. Ma, W. You and X. Zhan, *Adv. Mater.*, 2017, **29**, 1702125.
17. H. Lai, H. Chen, J. Zhou, J. Qu, P. Chao, T. Liu, X. Chang, N. Zheng, Z. Xie and F. He, *iScience*, 2019, **17**, 302-314.
18. R. Geng, X. Song, H. Feng, J. Yu, M. Zhang, N. Gasparini, Z. Zhang, F. Liu, D. Baran and W. Tang, *ACS Energy Lett.*, 2019, **4**, 763-770.
19. C. Li, H. Fu, T. Xia and Y. Sun, *Adv. Energy Mater.*, 2019, **9**, 1900999.
20. H. Lai, H. Chen, J. Zhou, J. Qu, M. Wang, W. Xie, Z. Xie and F. He, *J. Phys. Chem. Lett.*, 2019, **10**, 4737-4743.
21. X. Ouyang, R. Peng, L. Ai, X. Zhang and Z. Ge, *Nat. Photonics*, 2015, **9**, 520-524.

22. H. Li, Z. Xiao, L. Ding and J. Wang, *Sci. Bull.*, 2018, **63**, 340-342.

23. L. Yang, Z. Hu, Z. Zhang, J. Cao, H. Wang, J. Yu, F. Zhang and W. Tang, *J. Mater. Chem. A*, 2020, DIO: 10.1039/D0TA00651C.

24. C. Li, T. Xia, J. Song, H. Fu, H. Ryu, K. Weng, L. Ye, H. Y. Woo and Y. Sun, *J. Mater. Chem. A*, 2019, **7**, 1435-1441.

25. S. Feng, C. Zhang, Y. Liu, Z. Bi, Z. Zhang, X. Xu, W. Ma and Z. Bo, *Adv. Mater.*, 2017, **29**, 1703527.

26. Q. Zhu, D. Liu, Z. Lu, C. Gu, K. Zhang, X. Bao, Q. Li and R. Yang, *J. Mater. Chem. A*, 2019, **7**, 4823-4828.

27. H. Lai, H. Chen, Y. Shen, M. Wang, P. Chao, W. Xie, J. Qu, B. Yang and F. He, *ACS Appl. Energy Mater.*, 2019, **2**, 7663-7669.

28. J. Song, M. Li, Y. Zhou, J. Zhang and Z. Bo, *J. Mater. Chem. A*, 2019, **7**, 8889-8896.

29. W. Gao, T. Liu, C. Zhong, G. Zhang, Y. Zhang, R. Ming, L. Zhang, J. Xin, K. Wu, Y. Guo, W. Ma, H. Yan, Y. Liu and C. Yang, *ACS Energy Lett.*, 2018, **3**, 1760-1768.

30. C. Huang, X. Liao, K. Gao, L. Zuo, F. Lin, X. Shi, C.-Z. Li, H. Liu, X. Li, F. Liu, Y. Chen, H. Chen and A. K. Y. Jen, *Chem. Mater.*, 2018, **30**, 5429-5434.

31. J. Zhang, W. Liu, M. Zhang, Y. Liu, G. Zhou, S. Xu, F. Zhang, H. Zhu, F. Liu and X. Zhu, *iScience*, 2019, **19**, 883-893.

32. J. Qu, Q. Zhao, J. Zhou, H. Lai, T. Liu, D. Li, W. Chen, Z. Xie and F. He, *Chem. Mater.*, 2019, **31**, 1664-1671.

33. J. Qu, H. Chen, J. Zhou, H. Lai, T. Liu, P. Chao, D. Li, Z. Xie, F. He and Y. Ma, *ACS Appl. Mater. Interfaces*, 2018, **10**, 39992-40000.

34. H. Lai, Q. Zhao, Z. Chen, H. Chen, P. Chao, Y. Zhu, Y. Lang, N. Zhen, D. Mo, Y. Zhang, and F. He, *Joule*, 2020, **4**, 688-700.

35. Y. Cui, H. Yao, J. Zhang, T. Zhang, Y. Wang, L. Hong, K. Xian, B. Xu, S. Zhang, J. Peng, Z. Wei, F.

Gao and J. Hou, *Nat. Commun.*, 2019, **10**, 2515.

36. J. Wang, J. Zhang, Y. Xiao, T. Xiao, R. Zhu, C. Yan, Y. Fu, G. Lu, X. Lu, S. R. Marder and X. Zhan, *J. Am. Chem. Soc*, 2018, **140**, 9140-9147.

37. Y. Lin, Y. Firdaus, M. I. Nugraha, F. Liu, S. Karuthedath, A. ‐ H. Emwas, W. Zhang, A. Seitkhan, M. Neophytou, H. Faber, E. Yengel, I. McCulloch, L. Tsetseris, F. Laquai, T. D. Anthopoulos, Adv. Sci., 2020, 7, 1903419.

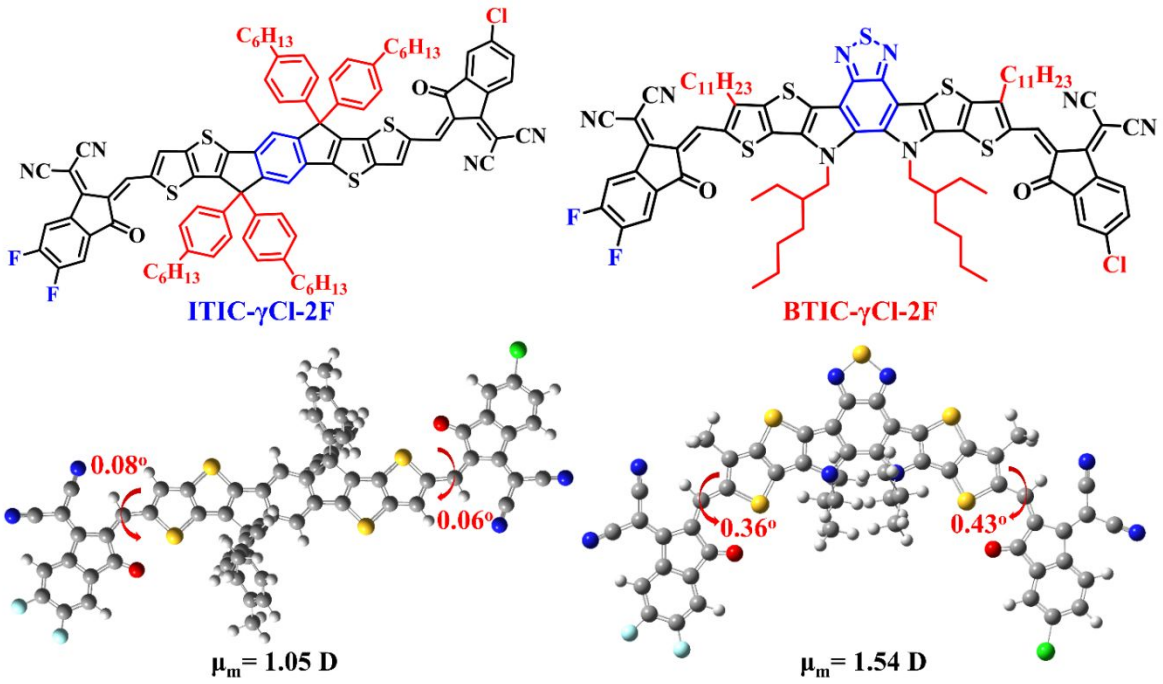

Figure 1. The structure and calculated molecular configuration for **ITIC-γCl-2F** and **BTIC-γCl-2F**.

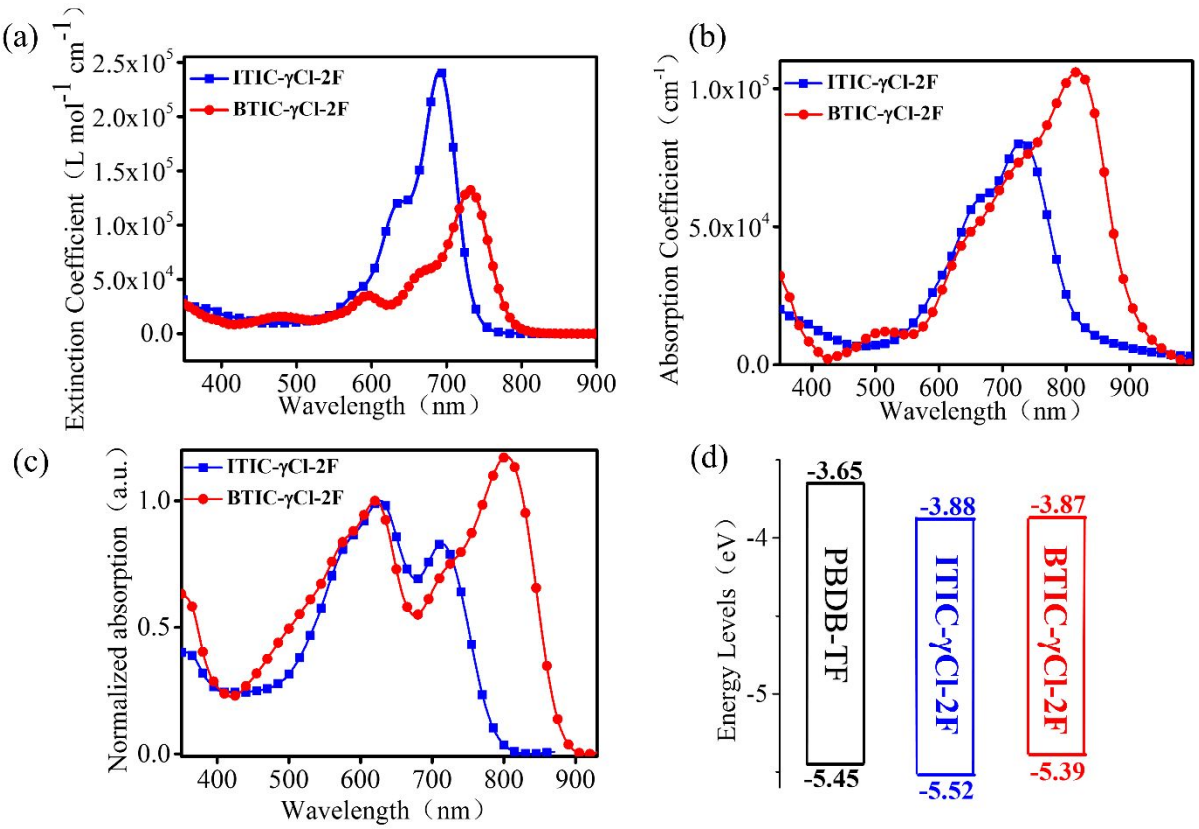

Figure 2. (a) The solution absorption, (b) film absorption, (c) blend film absorption spectra, and (d) the energy levels for PBDB-TF, **ITIC-γCl-2F** and **BTIC-γCl-2F**.

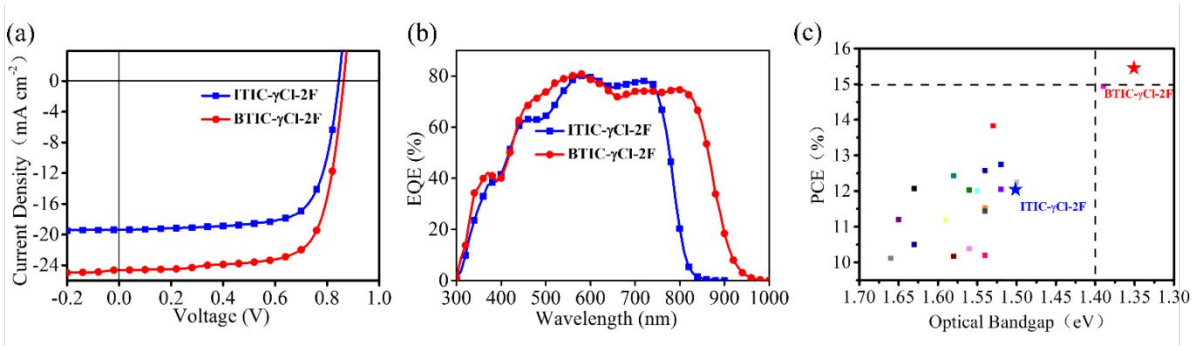

Figure 3. (a) The *J-V* curves and (b) the EQE curves for **ITIC-γCl-2F** and **BTIC-γCl-2F** (c) PCEs of over 10% based on the use of asymmetrical FREAs.

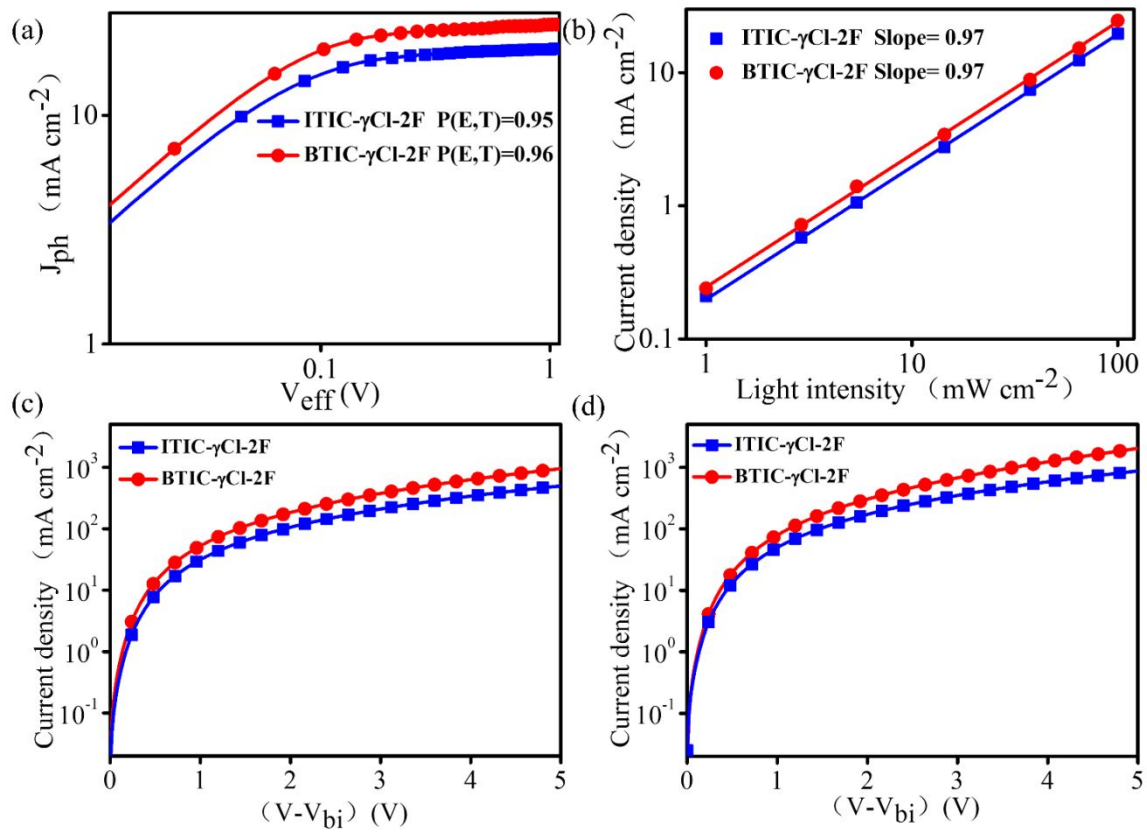

Figure 4. (a) The charge dissociation curves, (b) bimolecular recombination curves, (c) electron and (d) hole mobilities for **ITIC-γCl-2F** and **BTIC-γCl-2F**.

Table 1. Photovoltaic performance of two asymmetrical FREA-based OSC devices [a].

Acceptors	V_{OC} (V)	J_{SC} (mA cm^{-2})	FF (%)	PCE_{max} (%)	μ_h (cm^2 V^{-1} s^{-1})	μ_e (cm^2 V^{-1} s^{-1})	μ_e/μ_h
ITIC-γCl-2F[b]	0.85	19.60	72.20	12.02	1.7×10^{-4}	1.2×10^{-4}	1.5
	(0.85±0.001)	(19.14±0.14)	(71.68±0.40)	(11.83±0.14)			
BTIC-γCl-2F[c]	0.86	24.60	72.67	15.43	2.6×10^{-4}	1.8×10^{-4}	1.4
	(0.86±0.001)	(24.38±0.12)	(71.96±0.55)	(15.10±0.19)			

[a] Average data are obtained from 10 devices. [b] In CB, with DIO (0.5% volume). [c] In CF, with CN (0.5% volume).

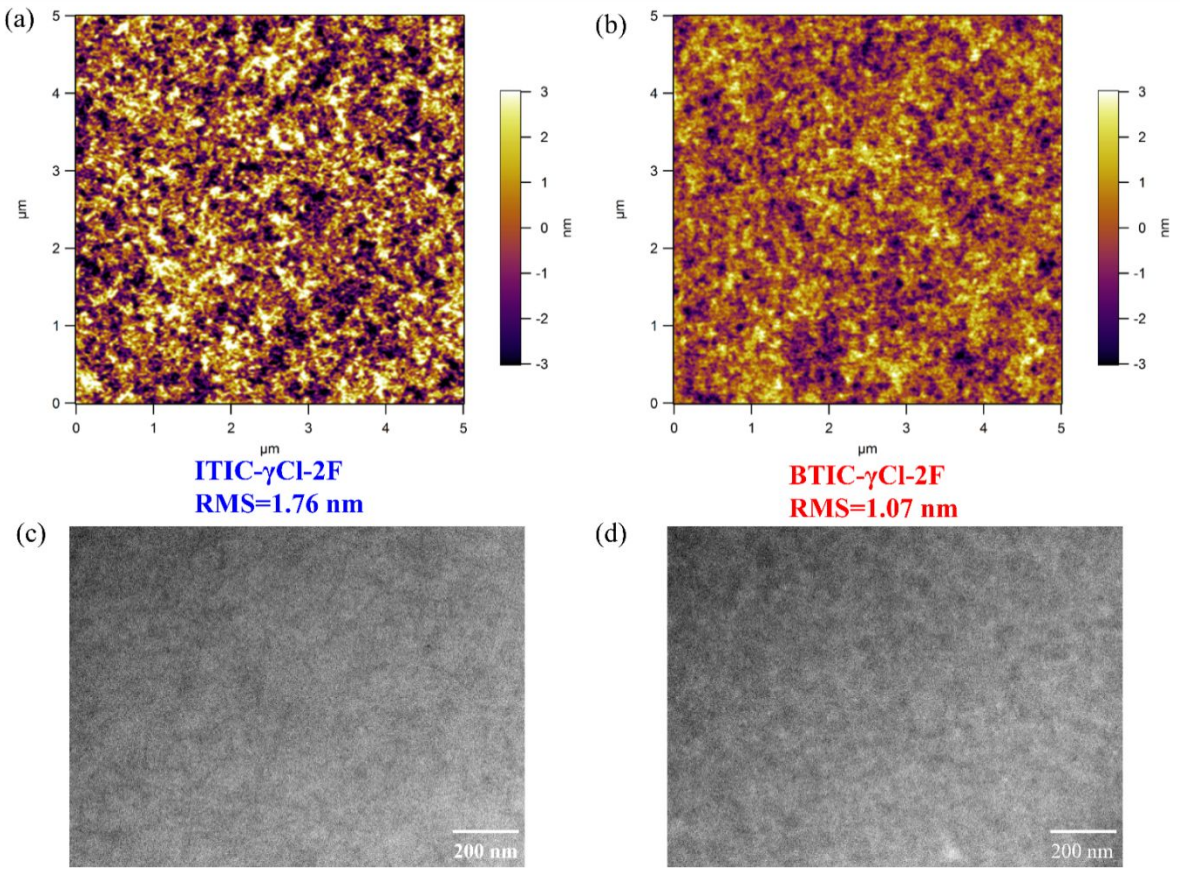

Figure 5. AFM images of (a) **ITIC-γCl-2F** (b) **BTIC-γCl-2F**; TEM images of (c) **ITIC-γCl-2F** (d) **BTIC-γCl-2F**.